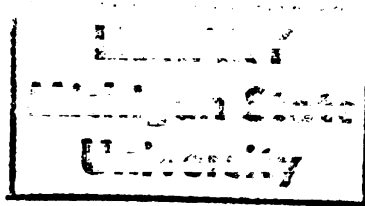




124
519
THS



This is to certify that the
thesis entitled
INHIBITING CORROSION CRACKING:
MICROSTRAIN AT THE CRACK TIP

presented by

ERIC B. SCHAPER

has been accepted towards fulfillment
of the requirements for

M.S. degree in MATERIALS SCIENCE.

A handwritten signature in cursive script, reading "Robert Sumner".

Major professor

Date 16 May 1986



RETURNING MATERIALS:

Place in book drop to
remove this checkout from
your record. FINES will
be charged if book is
returned after the date
stamped below.

--	--	--

**INHIBITING CORROSION CRACKING:
MICROSTRAIN AT THE CRACK TIP**

by

Eric B. Schaper

A THESIS

Submitted to

**Michigan State University
in partial fulfillment of the
requirements for the degree of**

MASTERS OF SCIENCE

Department of Metallurgy, Mechanics, and Materials Science

1986

Abstract

Inhibiting Corrosion Cracking:
Microstrain at the Crack Tip

by

Eric B. Schaper

To establish a corrosion fatigue testing apparatus capable of obtaining accurate values of crack growth rate and stress intensity (from crack length, load, specimen geometry and the number of cycles). Then the effects of adding a corrosion fatigue inhibitor to the environment of a specimen with a crack growing in the presence of distilled water were studied.

DEDICATION

To my parents, Helen and Earl Schaper, for their constant support and encouragement.

Acknowledgments

I would like to thank Dr. Robert Summitt for all of his guidance and patience during my graduate research. I would also like to thank the Department of Mechanics, Metallurgy, and Materials Science, and the Office of Naval Research for their help and financial assistance.

Table of Contents

Introduction	1
1.0 Corrosion Fatigue	1
2.0 Inhibitor	2
3.0 Background Work	7
Inhibitor Development	7
Inhibitor Research at MSU	13
Previous Research	14
Ongoing Research	16
4.0 Experiment	19
4.1 Preparation	19
Lab Set-up and Equipment	20
Specimen Design	24
Grip Design	25
Chamber Design	28
Cathetometer	30
Pretesting	32
4.2 Method	32
Mechanical analysis	32
Conditions	36
Precracking	36
Experimental	37
Specimen Preparation	38
Precracking Procedure	38
Chamber Mounting	39
Solution Preparation	39
Experimental Procedure	40
Introduction of Inhibitors	41
Test Termination	42
5.0 Data	42
Data Conversion and Calculations	42
Data	43
Discussion of the Data	46
SEM Evaluation	47
6.0 Conclusions	50
Bibliography	51

List of Tables

2.1	Inhibitor Formulation.	6
3.1	Variables considered during screening of the inhibitors.	8
3.2	Inhibitors under current evaluation.	16
4.1	Equipment List.	21
4.2	Composition of 7075-T651.	24
4.3	Precrack conditions.	37
4.4	Experimental conditions	38
4.5	Precrack Conditions	38
4.6	Inhibitor composition.	40
4.7	Experimental conditions.	41

List of Figures

3.1	Comparitve CF rates for 7075-T6.	10
3.2	Comparitve CF rates for 7075-T6, with inhibitor.	11
3.3	Khobaib's CF test replacing 0.1M NaCl with inhibitor	12
4.1	This plot shows the three portions of da/dN vs. K_I curve.	20
4.2	The basic layout of the hydraulic system and controllers.	21
4.3	Basic wiring Layout.	23
4.4	The MSU Compact Tension Specimen.	25
4.5	Grip assembly with CTS mounted.	26
4.6	Grip Dimensions.	27
4.7	Environmental chambers 1 and 2.	29
4.8	Placement of the environmental chamber on the CTS.	29
4.9a	Cathetometer Head.	31
4.9b	Load frame with cathetometer mounting apparatus.	31
4.10	The Wright-Patterson Compact Tension Specimen.	33
4.11	Wright-Patterson CTS.	33
4.12	MSU Compact Tension Specimen.	34
4.13	MSU Compact Tension specimen.	35
5.1	da/dN vs K_I plot for test No. 1.	44
5.2	da/dN vs K_I plot for test No. 2.	45
5.3	da/dN vs K_I plot for test No. 3.	46
5.4	CF fracture sufrace without inhibitor 750x.	48
5.5	CF fracture surface without inhibitor 500x.	48
5.6	CF fracture surface in the presence of inhibitor 1000x.	49
5.7	CF fracture surface in the presence of inhibitor 500x	49

Introduction

Corrosion fatigue (CF), and crack tip chemistry are the result of numerous processes all occurring simultaneously to bring about accelerated corrosion. If chemistry at the crack tip is modified, the fatigue crack growth rate can increase or decrease. Finding ways to inhibit CF involves the understanding of both the mechanisms by which CF occurs and how the inhibitors used affect the environment at the crack tip.

This report will cover the following topics:

(1) The causes of CF and stress corrosion cracking (SCC). A discussion of the mechanisms through which the environment at the crack tip affects the crack growth rate of fatiguing metal.

(2) How the inhibitor used in the experimental part of this investigation affects the crack tip chemistry and the fatigue crack growth rate.

(3) Previous and on-going work that is relevant to this investigation.

(4) The experimental section will cover both assembly of the fatigue testing apparatus and the experiments run.

(5) Discussion of the data and the conclusions from the results.

1.0 Corrosion Fatigue

The causes of corrosion fatigue and stress corrosion cracking, in aluminum, are believed to be the result of a localized aggressive cell at the crack tip. If the aggressive cell at the crack tip were to be eliminated or the negative effects inhibited, the crack growth rate could be reduced. Because the crack tip is isolated from the majority of the material, unique electro-chemical and mechanical conditions occur that do not occur elsewhere. Because of the inaccessibility of the crack tip to direct measurement or observation, there is little experimental data to substantiate present theories.

The following paragraphs attempt to define the theoretical mechanisms by which accelerated crack growth occurs.

There are three basic corrosion mechanisms that occur inside of a crack: differential aeration, localized acidification, and migration of chloride ions or other aggressive species (not extremely relevant,

because the tests were run in a chloride free solution of distilled water)
24.

When differential aeration occurs the system involves a large aerated area and a very small anaerobic area with an electrolyte connecting the two. For most common metals the presence of air promotes the formation of a film which would normally slow the corrosion process. In the restricted anaerobic areas, however, the film is weak and unstable, hence likely to be damaged by a high anion concentration. This causes the current density of the anaerobic area, such as a crack tip, to be much greater than the current density of the aerated area. Consequently, the attack is more rapid where the metal surface is isolated from oxygen²⁵. As a result the anodic dissolution mechanism causes the electrochemical potential to be more active at the crack tip than at the bulk of the material. Because of the potential difference between the crack tip and the outside surface, the electro-chemical driving force allows the system to become more favorable for corrosion at the crack tip [Omura].

Additionally, it is suggested that as a result of electro-chemical-mechanical action, the plastically deformed areas of the crack tip form an anode, and undeformed areas form a cathode⁹. This would further localize the cell at the deformed areas which exist predominantly at crack tip on the newly deformed metal.

The effects of localized acidification are the result of a drop in pH inside the crack tip resulting from precipitation and hydrolysis equilibria of the corrosion products. Since access to the crack tip is impeded, the pH level within the crack is maintained, resulting in a concentration cell²⁰.

Hydrogen evolution leads to hydrogen-enhanced embrittlement²⁰. The transport of hydrogen is most likely the result of dislocation transport, effectively embrittling the crack tip vicinity. There are two theoretical methods for dislocation transport of hydrogen into the deforming metal at the crack tip. The first is through the "normal diffusion mechanism", and is "associated with a dense dislocation network at the crack tip"¹⁷.

The second method for dislocation transport of hydrogen is by a dislocation sweep-in mechanism. "The impurity elements are swept deeply into the material by the mobile dislocations. The transport distance for hydrogen can be extremely large."¹⁷ It is noted¹⁷ that for

hydrogen embrittled intergranular fracture of aluminum, hydrogen that is swept into the grain boundary interacts and localizes with the impurities at the grain boundary lowering the fracture resistance.

In the presence of aggressive ions, such as chloride ions, the unprotected metal surface will adsorb, preferentially the damaging ion species. Once lodged on the surface these ions are difficult to remove even in the presence of inhibitor²⁴. Because the above theories are only theories, the actual mechanisms by which a material undergoes accelerated crack growth because of the aggressive environment at the crack tip are not known.

2.0 Inhibitor

"SEM studies show that environment has a strong effect on the microplastic behavior at the tip of a fatigue crack."²¹ Khobaib observed that CF crack surfaces showed a brittle-shear mode of failure with little evidence of normal fatigue features (striations). In general, the inhibitor affects the environment at the crack tip through preferential adsorption of the inhibitor on the newly exposed metal at the crack tip. The inhibitor investigated in this report, a Borate-Nitrate based inhibitor, is adsorbed in preference to the aggressive ions (if any are present), forming a protective layer that shields the metal from both the aggressive elements as well as the aqueous environment. Rosenfeld wrote, "In the joint presence of an aggressive and a passivating ion, it is the passivating ion that is preferentially adsorbed in the competition for adsorption."^{*1} Once the inhibitor is adsorbed to form a protective layer, the surface of the metal is isolated from the aggressive ions forming the localized cell at the crack tip.

^{*1} I.L. Rosenfeld, I.K. Marshkoo, Corrosion 20, 115 t, 1964.

The inhibitor used in this investigation contains four different types of inhibitors:

1. Non-oxidising Passivator - sodium borate
2. Oxidising Passivators - sodium nitrite and sodium nitrate
3. Barrier Layer Formers- sodium metasilicate pentahydrate and sodium hexa-meta phosphate
4. Adsorbed Layer Former - MBT (sodium 2-mercaptobenzothiazole)

There are two categories of inhibitors, those that work to protect the surface of the metal, such as barrier layer forming inhibitors and those that work in the solution. Passivators (oxidizing and non-oxidizing inhibitors), conversion layer formers, and adsorbed layer formers are all barrier layer formers. Barrier layer formers are the most widely used type of inhibitor. They work by adhering to the metal surface and protecting it from attack. Passivators are useful in aqueous solutions in the neutral range. These inhibitors shift the electrochemical potential of the corroding metal to a region where a stable insoluble oxide or hydroxide layer forms to protect the metal surface.

Cohen notes⁷ that inorganic anodic inhibitors usually are either buffering agents or oxidizing anions. Buffering agents require oxygen⁷. Oxidizing anions are effective in the absence of oxygen, but are more effective in the presence of oxygen. Oxidizing anions or passivators (eg., nitrite), form a protective oxide film²⁴ which decreases the exchange current density. The exchange current density is lowered by reducing the electron concentration in the electrical double layer²⁶. Passivating inhibitors are inexpensive, effective at low concentrations,

and reduce the corrosion rates to low values ¹⁵.

Conversion layer formers, also barrier layer formers, form insoluble compounds on the metal surface without relying on the oxidation requirement of passivating inhibitors ¹⁵.

Adsorbed layer formers are adsorbed firmly to the corroding surface preventing either the anodic or cathodic reactions. Adsorbed layer formers can be classified as cathodic, anodic or neutral inhibitors. Cathodic adsorbed layer formers, shift the corrosion potential in the negative direction, and anodic adsorbed layer formers, shift the corrosion potential in the positive direction. In addition, adsorbed layer formers can be categorized as inhibiting either acid or neutral solutions.

MacDill AFB located on Tampa Bay, adjacent to Tampa, Florida, is surrounded on three sides by salt water. The aircraft stationed at MacDill AFB were constantly exposed to high amounts of salt precipitated onto the aircraft from the air. To extend the service life of the aircraft a clear water rinse facility was built to automatically wash the aircraft. However the rinse could wash salt into crevices allowing highly concentrate NaCl deposits to accumulate. The result could be accelerated crevice corrosion. The Borate-Nitrate inhibitor was selected, as will detailed in the inhibitor development section, to counter-act the affects of the accelerants deposited in crevices ²⁵.

Manufacture of the inhibitor was contracted to the Erny Supply Co., Tampa Florida. The inhibitor for this experiment was obtained from a batch mixed by the Erny Supply Co. The composition is as follows: ¹⁵

<u>Compound</u>	<u>Weight %</u>
Sodium Borate [Borax]	0.35
Sodium Nitrate	0.10
Sodium Nitrite	0.05
Metasilicate Pentahydrate	0.01
Sodium Meta-hexa Phosphate	0.002
<u>MBT</u>	<u>0.001</u>
Sum	0.513

Table [2.1] Inhibitor formulation.

Sodium borate is a non-oxidizing passivator. Borate, a weak base, causes the formation of a protective oxide layer by replacing adsorbed hydrogen on the surface of the metal. The adsorbed borate ions form a diffusion barrier to oxygen at the metal surface²⁰. This prevents the likelihood that oxygen will react with the hydrogen. Because of the increased oxygen concentration, oxygen will replace hydrogen at the cathodic sites resulting in the formation of a passive oxide film¹⁵.

Sodium nitrite and sodium nitrate are both oxidizing inhibitors. These two passivators shift the cathodic polarization curve in the positive direction, as a result form a stable, insoluble, oxide layer¹⁵. Rosenfeld suggests (in support) that sodium nitrite diverts a larger part of the surface from the anodic reaction and hence shifts the potential more strongly toward positive values than other inhibitors²².

The "Nitrate inhibitor competes with the aggressive ions (such as chloride ions) for surface sites; it does not cause metal dissolution itself, hence the nitrate acts to protect the freshly exposed surface from attack."²¹ The adsorption of the nitrite on the surface is followed by the evolution of ammonia NH_4 .

Also, "Anodic metal coatings (passivators) which form protective films, have generally been shown to be beneficial even when the film formed was ruptured"⁹. Because sodium nitrite is an anodic inhibitor, it renders the inhibitor more effective. If the film breaks, the nitrite continues to function until the rupture in the protective layer can heal itself. However, cathodic coatings can be effective only if the coating formed remains unbroken"⁹.

In addition, at low concentrations in solutions containing sodium

chloride or sodium sulfate, sodium nitrite accelerates corrosion for concentrations up to 0.08 gm/l. But at higher concentrations, it exerts a strong inhibitive effect with a maximum effectiveness at 0.2 gm/l. Essentially, when the sodium nitrite concentration is higher than the accelerant ion concentration the inhibitor is effective. If the concentration of sodium nitrite is lower than the concentration of accelerant, then corrosion occurs.

Sodium metasilicate pentahydrate and sodium meta-hexa phosphate are conversion layer formers. These two form an insoluble layer of aluminum-silicate $Al_2(SiO_3)_3$, and aluminum phosphate $AlPO_4$ respectively. Conversion layer formers will cause passivity when sufficient thickness has been achieved. Silicates are especially effective on aluminum alloys ¹⁵.

Sodium 2-mercaptobenzothiazole (MBT) is an adsorbed layer former. MBT is adsorbed onto the metal surface interfering with the cathodic reaction. This inhibits the reduction of H^+ at the cathode ¹⁵. Because MBT is organic and surface active, it is also considered a surfactant.

3.0 Background Work

3.1 Inhibitor Development

Research of CF, SCC, and crack tip chemistry, have stemmed from the efforts of the Air Force to develop an effective corrosion inhibitor for aircraft. The multifunctional inhibitors were to be low cost, nontoxic, as well as effective in preventing localized corrosion, accelerated crack growth, and general corrosion for both ferrous and nonferrous metals.

Development of the inhibitor was done at the Wright Patterson AFB research facility. The program ¹³ evaluated more than 400 inhibitor compounds for their effects on the various forms of corrosion on steel, copper, and aluminum. Certain inhibitors already known to inhibit CF, such as chromates, were of ecological concern. Such toxic or hazardous inhibitors had to be screened out. A series of tests were performed on the inhibitors considering the variables listed in Table [3.1].

Polarization (potentiodynamic polarization technique was used in accordance with ASTM standard G5-720, immersion and galvanic-coupling

testing was done by C. T. Lynch, F.W.Vahldiek, and M. Khobaib to determine the effectiveness of the candidate inhibitors in aggressive solutions (high chloride concentrations) as well as the water used in the rinse facility. Although weight loss was calculated for the immersion test specimens the primary factor was based on visual observation (the appearance of the specimen after immersion testing).

1. Multifunctional
 - Cathodic
 - Anodic
 - Chloride Adsorbers
 - Buffers
2. Solubility Range
3. Influence on Hydrogen Entry Rates
4. Toxicity
5. Cost

Table [3.1] Variables considered during screening of the inhibitors ¹⁷.

In addition, CF and static sustained-load tests were run. The static sustained-load to determine the effects the inhibitor had on SCC and K_{ISCC} (threshold stress intensity for SCC).

As a result of these investigations, a Borate-Nitrate based inhibitor (Sodium Borate [Borax] 0.35 wt. %, Sodium Nitrate 0.10 wt. %, Sodium Nitrite 0.05 wt. %, Metasilicate Pentahydrate 0.01 wt. %, Sodium Meta-hexa Phosphate 0.002 wt. %, MBT 0.001 wt. %, hereafter referred to as "the inhibitor", or the Borate-Nitrate inhibitor) was selected because of its excellent corrosion protecting capabilities for steel, aluminum, and copper alloys used in aircraft.

The previous research, most relevant to the experiments performed for this report, was done by Kohbaib at the Wright Patterson AFB Research Facility. His work concerned the effects that various environments, both inhibited and uninhibited, had on fatiguing 7075-T6 aluminum. Figure [3.1] shows the effect that air, distilled water, tap water and 0.1M NaCl solution had on the crack growth rate. The sodium

chloride solution proved to be the most damaging. In addition, the distilled water, such as would be used in our experiments, also had an adverse effect on the fatigue crack growth rate, though not as great as the 0.1M NaCl. Figure [3.2] shows the effect of adding the inhibitor to the distilled water and sodium chloride solution (compared with uninhibited crack growth in air). The inhibitor essentially negated the adverse effect of both the distilled water solution and the aggressive chloride solution.

To help determine the functionality of the inhibitor on a propagating crack in an aggressive environment, Kobaib ran a test in which a specimen was cycled in a 0.1M NaCl solution to region II (constant crack growth rate) of the da/dN vs. K_I plot. Once the crack growth rate had leveled-off to a semi-constant rate, the 0.1 NaCl solution was replaced by a standard concentration inhibitor solution. Figure [3.3] shows that when the inhibitor was added there was a dramatic decrease in crack growth rate, followed by a delayed return to normal corrosion fatigue crack growth behavior. It was also shown that when the 0.1 M NaCl solution was replaced by the inhibitor, the fatigue fracture surface went from a brittle mode of fracture to a ductile fracture mode (as would be exhibited in the presence of air). This demonstrated that the crack growth rate could be arrested and reduced drastically in an aggressive chloride environment. No experiment was run to see if this effect was also present in the presence of only distilled water, with no aggressive ions present.

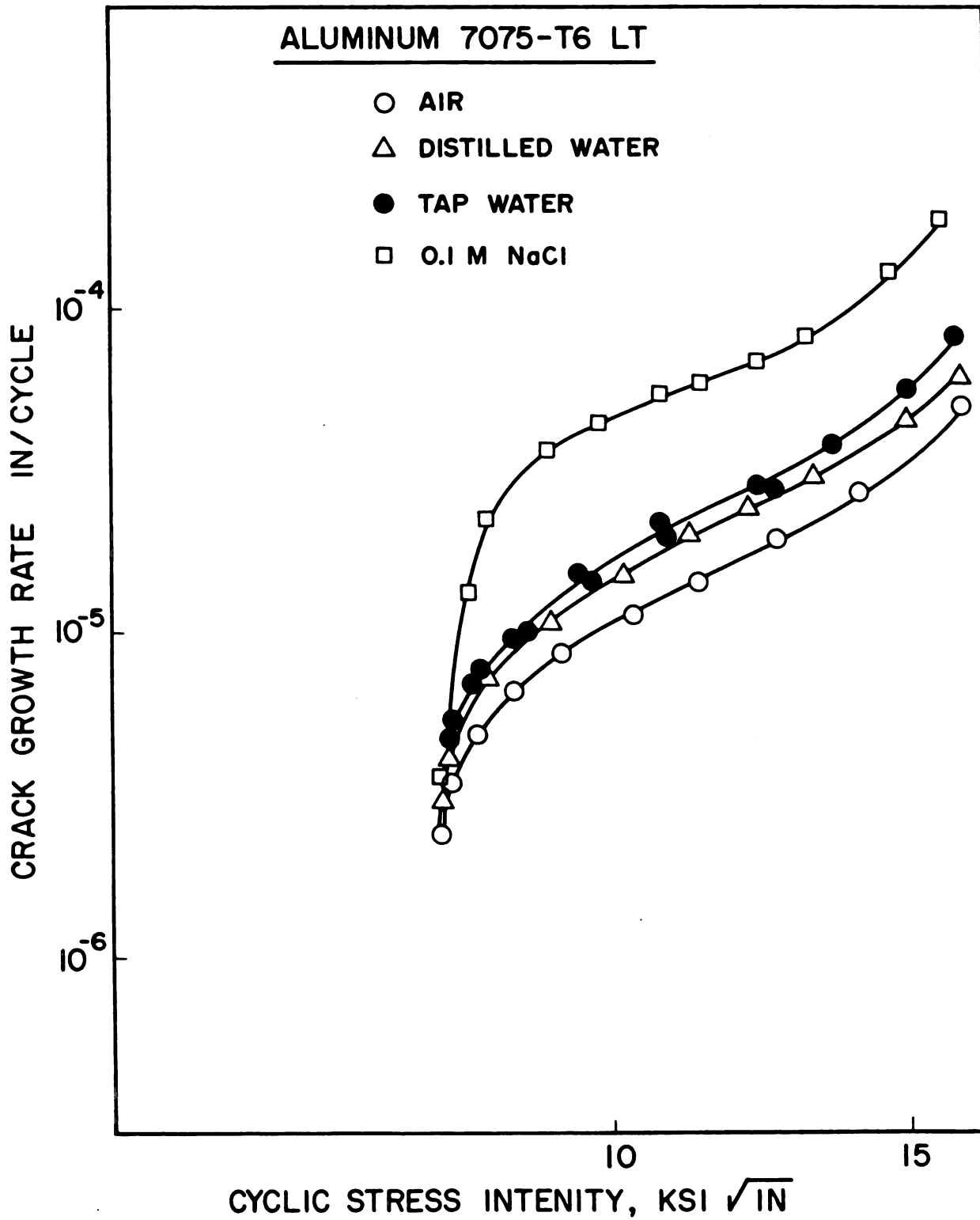


Figure [3.1] Comparative CF rates for Al 7075-T6 ¹⁴.

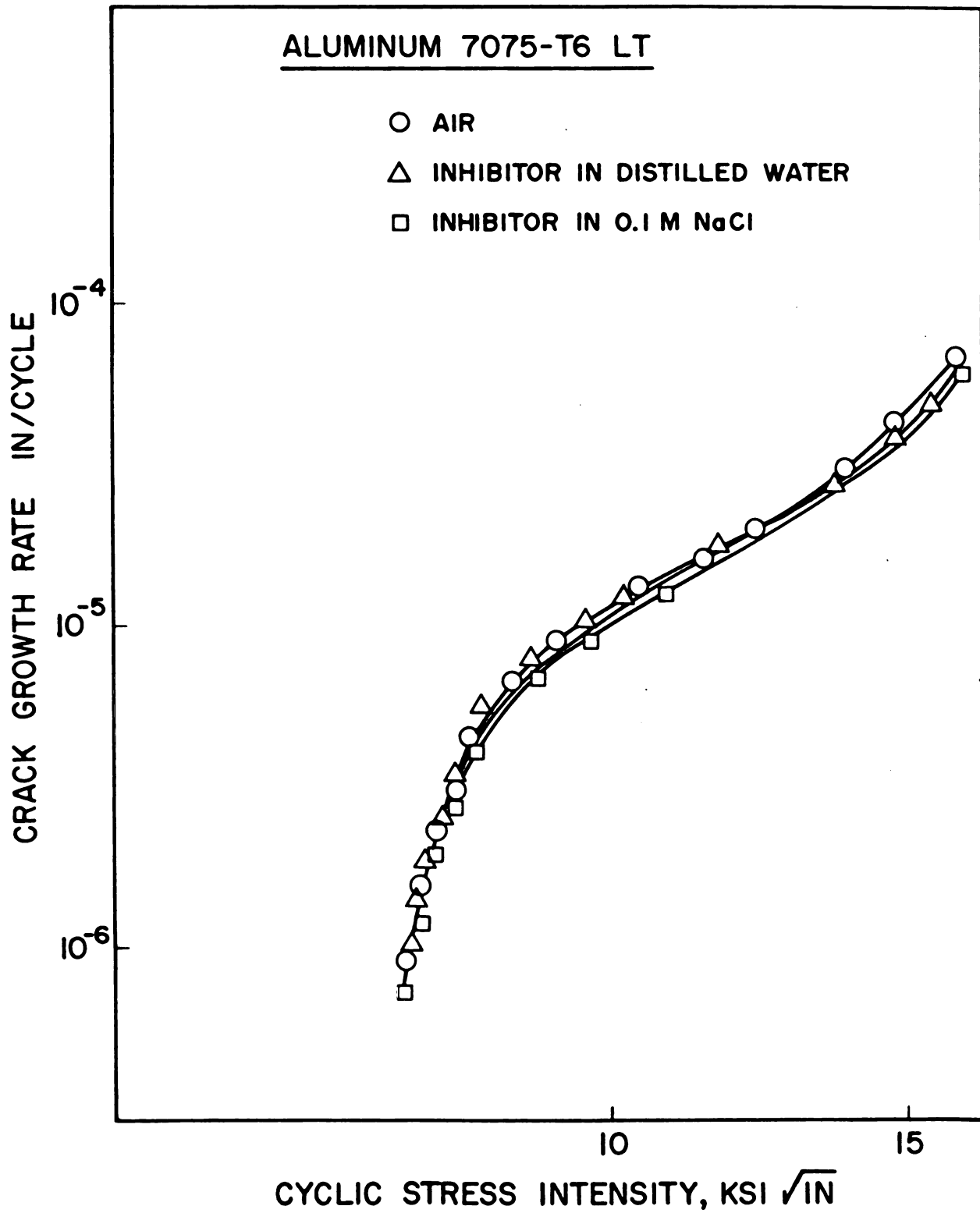


Figure [3.2] Comparative CF rates for Al 7075-T6, with inhibitor 14.

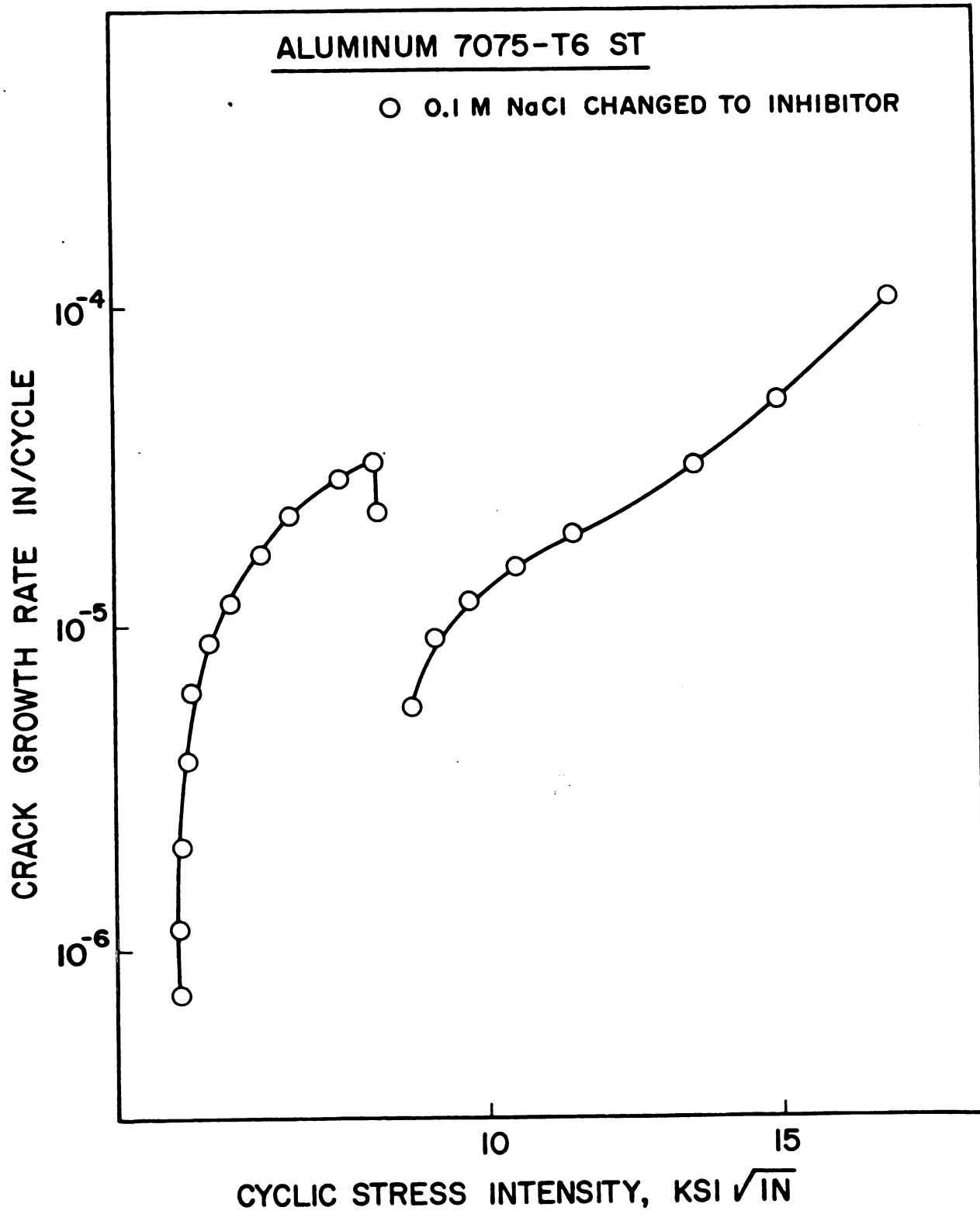


Figure [3.3] Khobalib's CF test replacing 0.1M NaCl with Inhibitor 14.

3.2 Inhibitor Research at Michigan State University

The research program at MSU, under the supervision of Dr. R. Summitt, has two paths of attack, that will attempt to perform key experiments evaluating theoretical models and resulting in practical advances in the ability to predict and control corrosion ²⁴.

The program empirically compares the electrochemical environment within a stressed crack and the crack propagation rate with external physicochemical conditions controlled by accelerants/inhibitors. Systematic variation of external environment and accelerant/inhibitor is explored.

The program will also investigate the chemistry and physics at the crack tip. Advances in the ability to measure conditions of pH, strain, and corrosion kinetics will enable theoretical concepts of corrosion crack growth mechanisms to be experimentally evaluated ²⁴.

Previous as well as on-going research at MSU has investigated the following topics:

Previous Research Topics 3.2a:

- The Effect of Multi-Functional Inhibitors on the Electrochemistry Within a Corrosion Crack - H. Omura Ph. D. (Dissertation)
- The effects of surfactants upon Corrosion Inhibition on 7075-T6 aluminum - Freddy Castellanos (Masters Thesis)
- Follow-up work on the PACER LIME algorithms and definition of inhibitor types and mechanisms
- Alternate immersion testing of inhibitor/accelerant systems.

On-Going Research Topics 3.2b:

- Additional evaluation using the electrochemical potentiodynamic polarization techniques to evaluate nitrogen oxyanion inhibitors.
- Evaluation of pH values within the crack tip using microelectrodes.
- Evaluation of the NaNO_2 concentration in an inhibitor/accelerant solutions, to determine the amount of reduced NaNO_2 relative to ratio of inhibitor to accelerant in the solution.

- Corrosion Fatigue testing of 7075-T651 Al, cycled in distilled water and followed by an introduction of the Borate-Nitrate inhibitor.
- Future testing will evaluate the stress-strain behavior over a few microns at the crack tip. This will be done with an interferometric (laser) strain gauge.

3.2 Previous Research Topics

Omura, researching the effect of multi-functional inhibitors on the electrochemistry within a corrosion crack, used electrochemical potentiodynamic polarization techniques to determine the following ²⁰:

- 1) The electrochemical and mass transport mechanism of 7075-T6 Al alloys between the crack tip and the bulk of the material.
- 2) The relation between the micro-electrochemistry and the environment outside of the crack, controlled by the inhibitor.
- 3) The relationship, in the presence of Cl^- , between the microchemistry at the crack tip and the bulk environment.

Polarization tests showed that increasing the corrosion current corresponds to increasing the Cl^- concentration, however, showed that as Cl^- concentration increased the corrosion potential decreased ²⁰.

Electrokinetic experiments were performed for coupled and isolated crevices. For the coupled crack, the anodic profiles showed that the dissolution rate inside the crack was much higher than the outside surface. It was also found that the cathodic reaction occurs at the outside surface and the anodic reaction and hydrogen reduction take place in the crack ²⁰.

Anodic profiles of isolated crevices showed that the dissolution rate inside the crack was much higher than on the outside surface. In addition, the pH and the polarization potential for the isolated crack were different than for the outside surface. The isolated crack experiments also showed that the rate of corrosion is controlled by the cathode reaction ²⁰.

Other effects that were observed at the crack tip were: accelerated dissolution due to restricted mass transport, the accumulation of electrolyte, the formation of anode(s), caused partially by the anaerobic (nonaerated) environment (with the bulk surface forming the aerated cathode) and weak acidity^{20,27}. It was also found that if the oxide film formed on the metal surface of the crack were to rupture, that the newly exposed metal would be subject to highly localized attack²⁰.

To investigate the conditions in a real crack, static-load tests were also done (using a WOL type specimen) to determine the effects stress had on the corrosion rate and the current density. The results of the static-load tests showed: the corrosion potential was moved 15mV in the active direction as a result of applied stress, an increase in current density, and it also showed that an applied stress affects the type of oxide film formed on the surface of the metal.

Omura's tests were also able to show that NaNO_2 at low concentrations was ineffective in passivating an aggressive Cl^- (1-3 wt. %) solution, but that a multifunctional inhibitor (the Borate-Nitrate inhibitor) was an "excellent" inhibitor²⁰. It is known that if oxidizing inhibitors (specifically nitrites) are added in insufficient quantities, they can accelerate the corrosion rate. Supplemental tests have shown that in the presence of Cl^- , nitrite, one of the components of the borax-nitrate inhibitor, is ineffective in preventing attack because of reduced cathodic polarization²⁴. The tests also showed hydrogen evolution in the crack leads to hydrogen embrittlement of the crack tip region. Omura also showed that the geometry of the crack played an important effect on the potential and pH gradients inside the crack.

The effect of surfactants on the performance of inhibitors was investigated by F. Castellanos⁶. The surfactants were tested with four inhibitor formulations all of which contained varying concentrations of the borate-nitrate inhibitor. Potentiodynamic polarization techniques were used to evaluate both the inhibitor-surfactant and surfactant systems in chloride solutions.

Surfactants, which include MBT, are organic substances which work by strengthening the adsorbed film on the surface. According to Vermilyea²⁴, surfactants become attached to Al_2O_3 by the inorganic group, resulting in a hydrophobic surface. Khobaib and Castellanos note that surfactants act synergistically with the borate-nitrate inhibitors to

form a stronger oxide film ²⁴.

Tests showed that at low concentrations of NaCl solution the the inhibitor-surfactant formulations were effective at providing protection from corrosion. The surfactants alone, were ineffective. When the concentration of the chloride solution was high the inhibitor-surfactant solutions were ineffective. There was no passivation resulting from the film that was formed at high chloride concentrations. The protection afforded by the surfactants increased with the concentration. Castellanos, as noted before, found that the borate-nitrate inhibitor acts synergistically with the surfactants.

Lenz defined both the type and the mechanism of inhibition, of different inhibitors. These definitions included detailed descriptions of performance of the constituents of the borate-nitrate inhibitor ¹⁵.

An alternate immersion testing system was assembled to test various inhibitors, surfactants, and inhibitor-surfactant system's effectiveness on surface corrosion. Both visual inspection of the specimens and weight loss measurements were used to evaluate the test solution performance as well as to determine the corrosion rate.

3.2b On-Going Research Topics

Currently, potentiodynamic polarization techniques are being used to evaluate components of the borate-nitrate inhibitor and alternate inhibitor compounds in a 0.1 wt.% NaCl solution. The compounds being evaluated are:

borate-nitrate inhibitor
 sodium hyponitrite
 ammonium hydroxide
 sodium nitrite
 sodium nitrate
 sodium nitrate + sodium borax

Table [3.2] Inhibitors under current evaluation.

The polarization tests are intended to determine the surface corrosion rate for the inhibitor formulations listed above. These experiments have not been completed.

Microelectrodes, to measure directly the pH inside of a crack, are being fabricated and calibrated. Microcapillary pipettes were heated and drawn to an outside diameter of $\approx 10\mu\text{m}$. The microelectrodes made from the drawn pipettes, are then inserted directly into a cyclicly grown crack in a compact tension specimen. The pH at various points in the crack can be measured and pH gradients can be determined experimentally.

Analysis of inhibitor/NaCl solutions is being done to determine the amount of nitrite in the Nitrate-Borate inhibitor that is being reduced. The NaNO_2 is varied from 1.0 wt. % to 0.06 wt. %, while the NaCl concentration is held constant at 0.1 wt. %. The solutions are tested for 14 days, after which time the solutions are tested using photospectrometry to determine the new NaNO_2 content.

Results have shown that at high nitrite concentrations the surface is occupied predominately by the nitrite and the nitrite reduction is low. At medium concentration of nitrite ion the boundary is shared with the chloride ions. The corrosion rate is high and the reduction of NaNO_2 is much higher. This is due to need of repair for the oxide film. At low concentrations of nitrite ion, the boundary is occupied predominately by the chloride ions. The low nitrite ion concentration on the surface leaves less film to be repair yielding a lower reduction of nitrite ions.

Microstrain measurements will be done with an interferometric strain guage. The strain is measure over a distance of only $100\mu\text{m}$. The interferometric strain guage uses a laser reflection off of a pair of Vickers hardness indentations to establish a fringe pattern (constructive and destructive interference) that can be converted into strain measurements. Because of the small guage length the strain, in the region experiencing the effects of the environment, at the tip of the growing crack can be measured.

Corrosion fatigue experiments, described in detail in this report, were performed on 7075-T651 Al compact tension specimens (CTS). The test was similar to khobaib's evaluation of the effects the

inhibitor had on a growing crack described in Materials Evaluation: Part II - Development of Corrosion Inhibitors. The inhibitor was added to a distilled water solution, instead of replacing a NaCl 0.1 wt.% solution. Omura's investigations are useful for explaining what was happening inside of the cyclicly growing crack. Because the growing fatigue crack is similar to the artificial and real cracks Omura investigated, several assumptions can be made about the fatigue crack (note the magnitude or form of the effects will not be the same as Omura's results, however, the trends will be similar):

1) The stress applied to the CTS in the CF will cause a shift in the active direction of the corrosion potential as well as raising the current density and altering the type of oxide layer formed.

2) Inside the crack an anaerobic anode will form and the outside surface will form a cathode. This will be the result of differential aeration. Both the pH and polarization potential will be different for the crack.

3) A rupture in the protective oxide layer formed by the inhibitor will cause a highly localized cell at the exposed metal surface.

4) Accelerated anodic dissolution will occur at the isolated crack tip as a result of the localized cell formed at the crack tip

5) Hydrogen evolution at the crack tip will allow hydrogen to diffuse by dislocation transport, into the metal ahead of the growing crack. The hydrogen in the crack tip region will weaken the metal causing hydrogen embrittlement.

6) It is worthwhile to note that NaNO_2 is ineffective in the presence of chloride ions. However, the CF tests in this report were run in distilled water, therefore, NaNO_2 will help to inhibit accelerated CF crack growth.

The Study of the effects of surfactants proved that inhibitor/surfactant compounds, ie., the inhibitor with MBT, can act synergistically to protect the metal surface. Castellanos, Khobaib, and Vermilyea agree that the surface active agents work to strengthen the protective oxide film formed by the inhibitor. Thus, the inhibitor is more effective.

Future Research At MSU

The ongoing experimental programs will systematically combine data from CF, polarization, alternate immersion, microstrain, and microelectrode profile testing. This program will give a better understanding of the mechanisms and performance of current and potential inhibitor formulations. The establishment of a CF testing capability at MSU provided a new method for evaluating inhibitor performance.

Polarization experiments will provide electrochemical profiles to facilitate better understanding of the electrochemical characteristics of inhibitor/surfactant/accelerant formulations. Alternate immersion testing will also provide data showing the physical effects that the inhibitors, surfactants, and accelerants have on surface corrosion. Microstrain and microelectrode development will enable evaluation of the crack tip environment. Both stress-strain and physicochemical, CF experiments will provide practical information on how well the inhibitors act to prevent accelerated crack growth.

The next step in CF research will be to evaluate the inhibitor in NaCl solution to confirm Khobalib's work. When the testing apparatus is capable of reproducing test data similar to Khobalib's, new inhibitor formulations can be tested. Comparative evaluation of inhibitor performance, to determine the protective qualities of the inhibitors against CF, would key information for inhibitor selection.

The repair and assembly of the cyclic testing system will benefit other research as well. The test specimens for the microelectrodes will be cyclicly cracked in the CF test system. In addition, the cyclic test system can be used, with the installation of a more capable function generator, to perform constant strain rate tests.

As a result of systematic experimentation, this program will hopefully provide answers to theoretical questions about accelerated crack growth as well as a way to prevent it.

Section 4.0 Corrosion Fatigue Experiment

4.1 Preparation

The experiment was run on a closed loop MTS hydraulic cyclic loading system. The experiment involved cyclicly loading a compact

tension specimen, made from 7075-T651 aluminum, in an aqueous environment into region II of the da/dN vs K_I plot (see Figure 4.1). Here the crack growth rate would be relatively constant. Once constant crack growth behavior was exhibited by the specimen, inhibitor was added to the environment. This would theoretically result in a decrease in the crack growth rate. The numerical data gathered was crack length, measured with a horizontal cathetometer, and the corresponding number of cycles. From the crack length, number of cycles, specimen geometry, and applied load, the crack growth per cycle [da/dN in m/cycle], vs stress intensity [K_I in $MPa\sqrt{m}$] could be plotted.

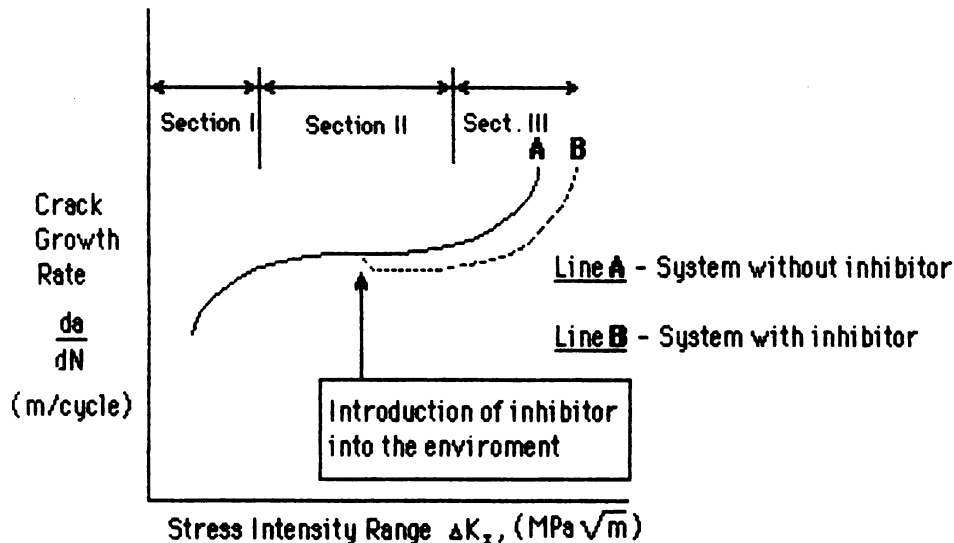


Figure [4.1] This plot shows the three portions of the da/dN vs. K_I curve.

4.1.1 Lab Set-up

The lab facilities and equipment used in this investigation were provided by the Department of Civil Engineering. The equipment provided had previously been used for cyclic testing of soil samples and was in a state of disrepair. The equipment also had to be converted for fatigue testing compact tension specimens.

To perform the corrosion fatigue tests the following equipment was used:

MTS Model 406.11 Controller
 MTS Model 436.11 Control Unit
 Strainert 25,000 lb. Load Cell
 MTS Mod. 206.11 - 11 Kip Hydraulic Actuator (ram)
 MTS Hydraulic Pump
 Digital Voltmeter

Table [4.1] Equipment List

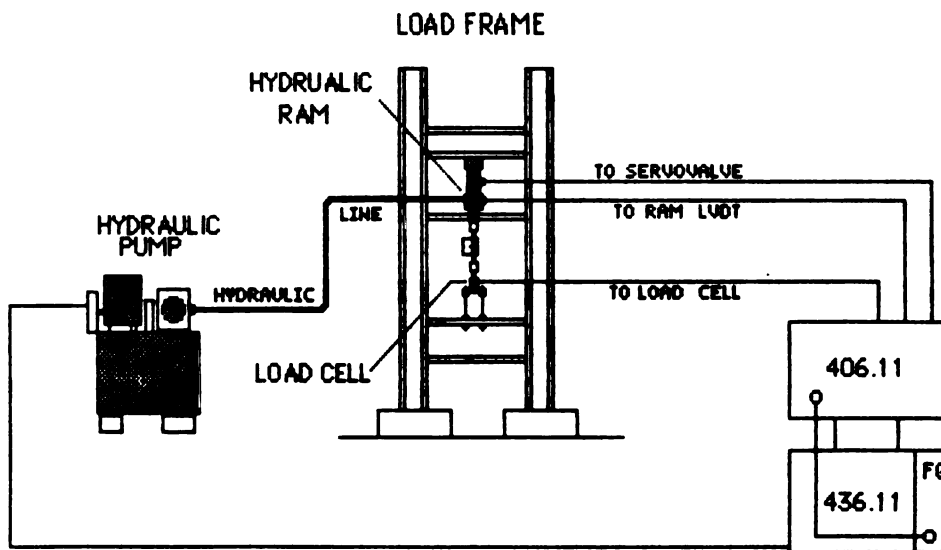


Figure [4.2] The basic layout of the hydraulic system and controllers.

The equipment was connected in a closed loop, so that the entire hydraulic system was controlled and calibrated by adjusting the MTS 406.11 and 436.11 controllers. The figure above [Figure 4.2.] shows a basic layout of the system. The digital voltmeter, not listed on the diagram, was connected to the 406.11 control unit to read the output voltage of the strainert load cell.

The MTS Systems Model 406.11 controller and 436.11 control unit were used to control the hydraulic pump. The pump pressure, in turn, controlled the load/stroke exerted by the hydraulic actuator (ram). The 406.11 controller had integral valve control and DC transducer options. The MTS 406.11 controller provided span, set point, and excitation controls to set the maximum, minimum and mean stress, as well as to calibrate the ram and the load cell. The DC transducer conditioner in the 406.11 unit was connected to the load cell (a DC transducer), thus allowing the experiment to run under load control.

The excitation of the DC transducer conditioner was calculated as specified in the calibration instructions in the operation manual. The excitation was set for a $\pm 5V$ range, for the load cell sensitivity of $3mV/V$. The $\pm 5V$ range was chosen by suggestion from Dr. John Martin and Joe Marksteiner. The MTS controllers were designed to operate on a $\pm 10V$ range. However, Dr. Martin had noted the accuracy and performance at the outer limits of the range of MTS controllers to be inadequate. Therefore, the $\pm 5V$ range was selected to eliminated possible error.

The 436.11 control unit was equipped with an integral MTS model 436.11FG function generator. This provided both waveform and frequency controls. A frequency of 2 Hz, and a sinusoidal wave were selected.

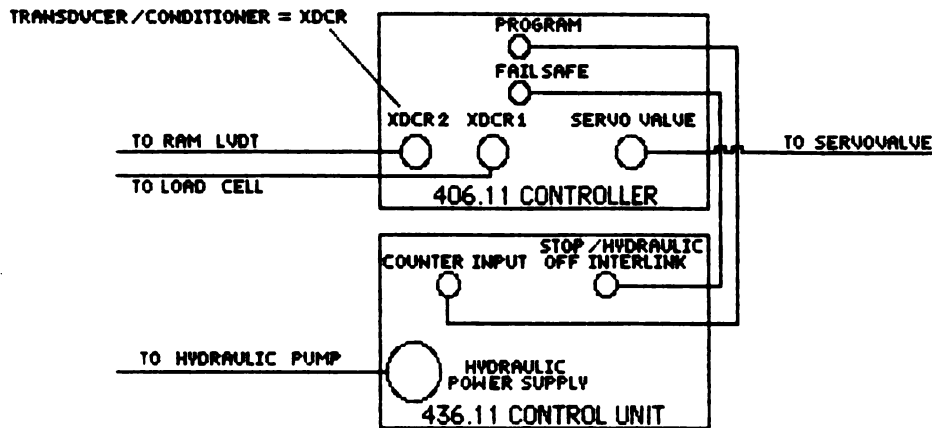


Figure [4.3] Basic wiring layout.

The load cell was a Strainert 25000 lb. load cell with a sensitivity of 3mV/V. The load cell was mounted on a platform opposing the hydraulic ram. The platform, provided by the Department of Civil Engineering, consisted of four posts supporting a plate to which the load cell was attached. The platform's four posts were bolted to the load frame.

To be compatible with the MTS 406.11 controller, the load cell had to have the jack connecting the two units replaced. However, when the jack was replaced, it was discovered that the load cell was wired incorrectly. The load cell was completely rewired. The problem of improperly wired cables connecting various parts of the system was very common. Several of the other cables had to be either rewired or completely rebuilt.

The system was calibrated to the load cell, as detailed in the operation manual, using a proving ring. When the load cell was properly calibrated, the ring would yield displacement values that maintained linear uniformity for a plot of load vs. voltage. The linear uniformity of the load vs. voltage was maintained well beyond the range needed for the experiment. A ratio of 4.2×10^{-4} Volts/lb was obtained from calibration.

The linear uniformity was established by comparing the readout on a digital voltmeter to a function of the displacement of the proving ring. The calibrated proving ring was provided with data that allowed conversion of the displacement of the ring to the load [in lbs.] exerted on

the ring. This could in turn be compared to the output voltage that induced the actuator to produce the resultant load. Then over a range of voltages, increased in linear increments, the controller can be calibrated to yield a series of linear increases in the resultant load. In addition, the system had to be zeroed so that 0.0V corresponded to a zero load.

After assembling a working hydraulic load frame, the specimen had to be designed, and the remaining parts of the apparatus designed and assembled. Additional equipment used included: the grips, an environmental chamber, and a vertical cathetometer converted to a horizontal cathetometer. All of these pieces of equipment had to be altered or fabricated for this experiment.

4.12 Specimen Design

Compact tension specimens were machined from a plate of 7075-T651 Al.

Element	%
Zn	5.5
Mg	2.8
Cu	1.4
Cr	0.2
Al	Remainder

Table [4.2] Composition of Al 7075-T651.

The compact tension specimen (CTS) design was selected from a group of candidate specimens after consultation with Dr. Summitt. Specimens under consideration were: the specimen used at the Wright-Patterson AFB facility, two ASTM standard specimens (note: the specimen designs listed in the ASTM standards gave tolerances. The two ASTM specimens fit two different specifications), and the "MSU specimen", a CTS design that had been previously used at MSU. The MSU CTS (Figure [4.4]) was chosen.

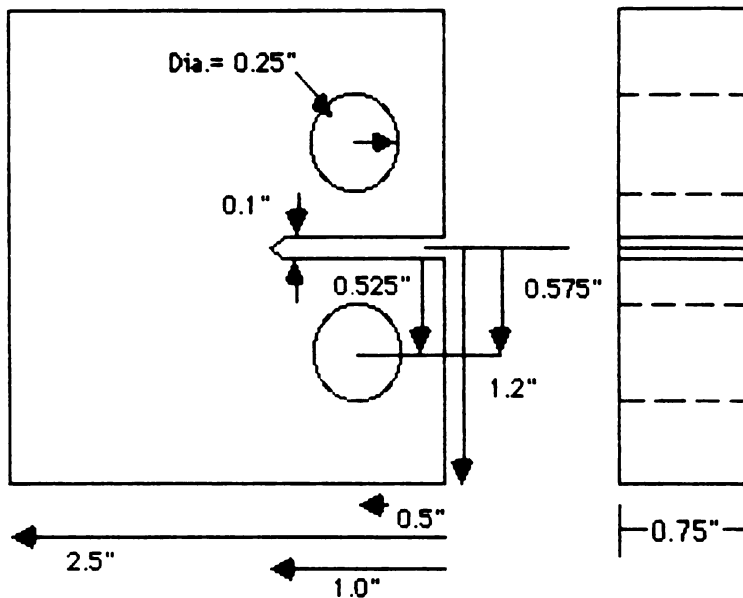


Figure [4.4] The "MSU Compact Tension Specimen.

4.13 Grip design

The grips were designed for tension-tension testing. The grips consisted of two pair of clevises, one pair from the bottom grip and another pair from the top grip, both pinned to the specimen. The grips were screwed to the load cell and the hydraulic ram. To facilitate future testing, the grips were designed to accommodate both 0.75" thick and 1.0" thick specimens. To change the grips to accommodate different specimen thickness, the clevises were inverted.

The grips were machined from stainless steel and the dimension are given in Figure [4.6]. Not shown, are four 0.5" stainless steel pins used to attach the specimen to the clevises.

26

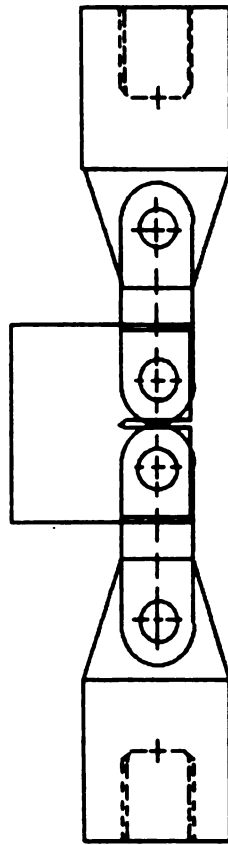
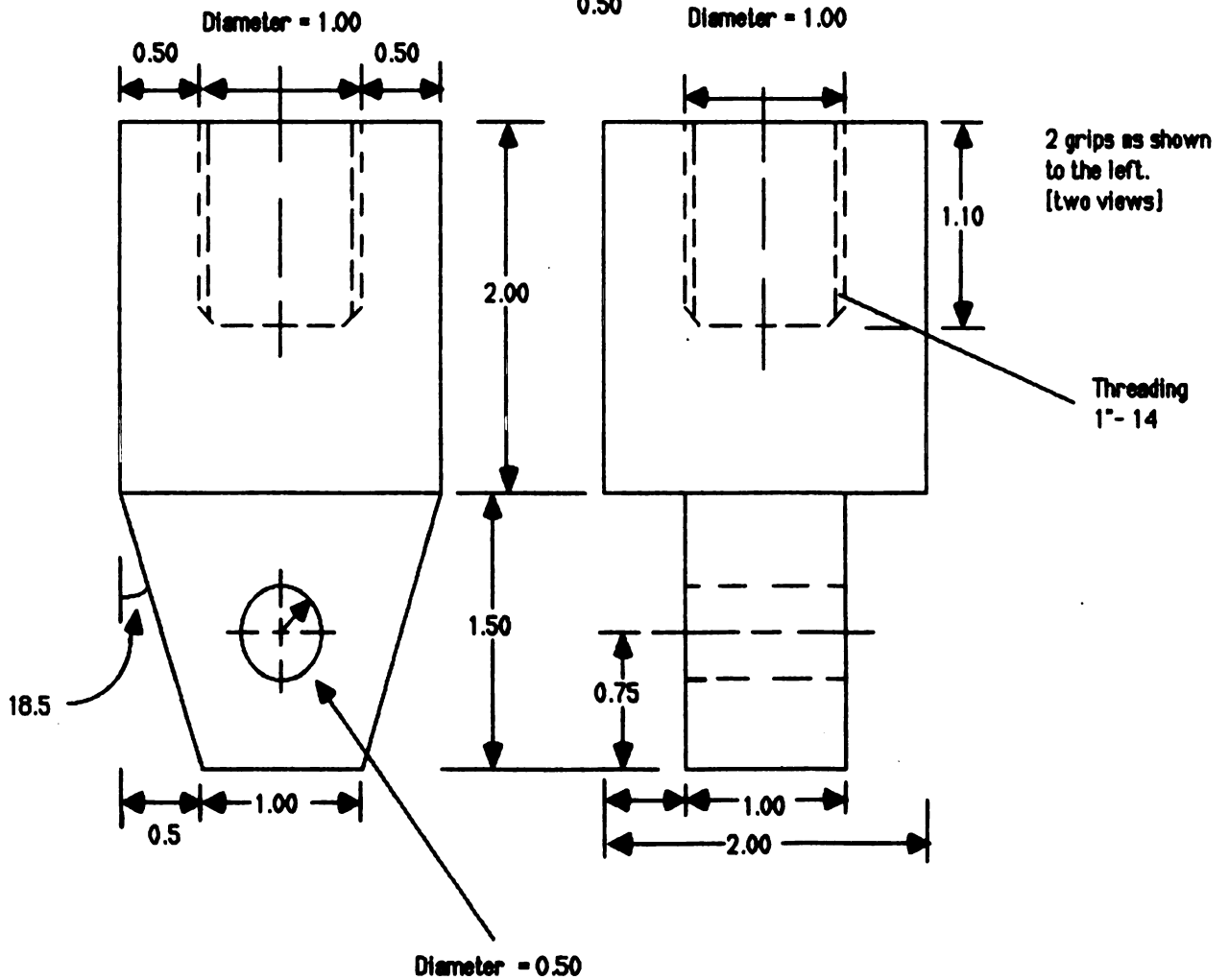
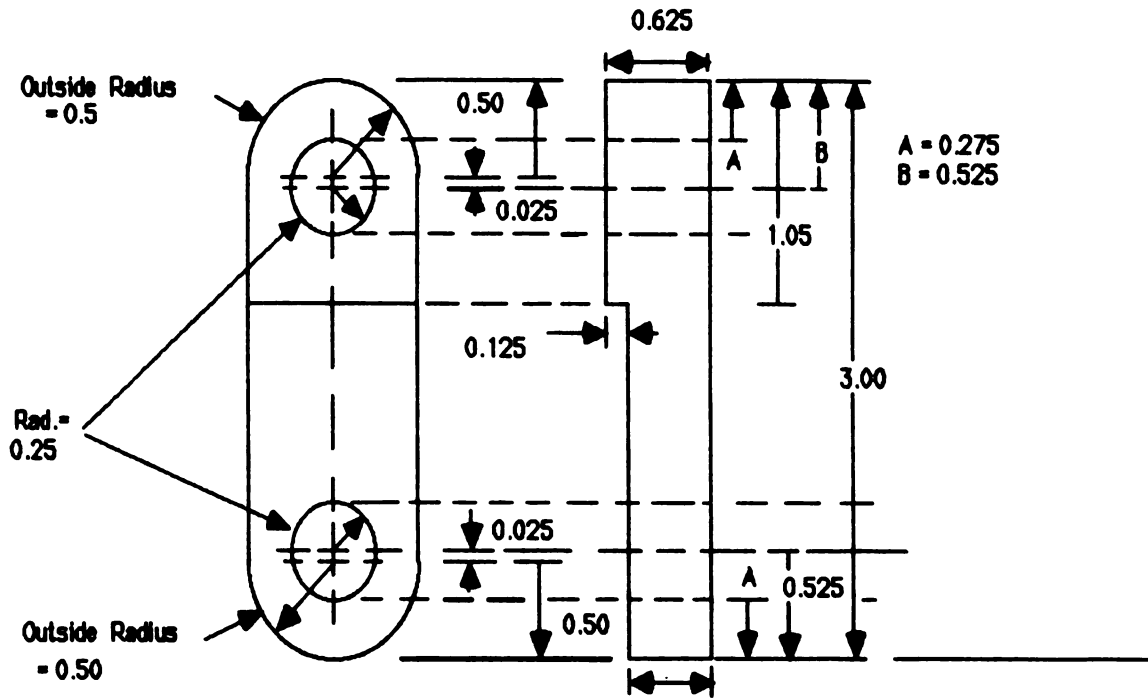


Figure [4.5] Grip assembly with CTS mounted.

Figure [4.6] Grip dimensions(Following page).

All dimensions are given in inches .

4 plates of the below cross section .



4.14 Chamber design

An environmental chamber was affixed to the specimen to provide a way in which the crack could be exposed to specific conditions or chemicals (corroding agents or inhibiting agents) that could be maintained at constant levels throughout the experiment. Initial planning was for an environmental chamber that included enclosing the entire specimen. However, cost and complexity of creating a workable version of this chamber was too high. The next concept was to glue a small chamber onto the side of the specimen where the crack was to propagate, thus exposing only the crack and a small area around it to the test environment.

To affix the chamber to the side of the specimen Dow Corning silicone sealant was used. Silicon sealant was chosen because it provided an excellent water tight seal. In addition, because of its rubber like properties, the seal did not degenerate during cycling, nor did it break its seal with the surface when the crack opening displacement grew large as the experiment proceeded. Once attached to the specimen, the distilled water or the inhibitor could be injected into the chamber with a hypodermic syringe.

The first chamber designed involved a 3/4" plastic tube sealed to the specimen at one end, sealed with a cover slip at the other end. A silicone sealant syringe port was used to for access for the hypodermic (see chamber 1, in Figure [4.7] below). During trial testing this chamber's durability to multiple uses or even multiple injections proved to be poor. In addition, the glass cover slip often cracked while the specimen was being mounted in the grips, and the silicone sealant syringe port leaked.

Chamber 2 (see chamber 2, in Figure 4.7 below) was similar to chamber 1. The glass cover slip was replaced with a rigid polystyrene sheet, and the silicone sealant syringe port was replaced with a vaccine bottle top (literally broken off the top of a vaccine bottle). The plastic sheet proved to be much more resilient to specimen mounting. The vaccine bottle top also worked without any problems of leaking or durability to multiple injections. Chamber 2 was used for all three of the experiments in which data was gathered.

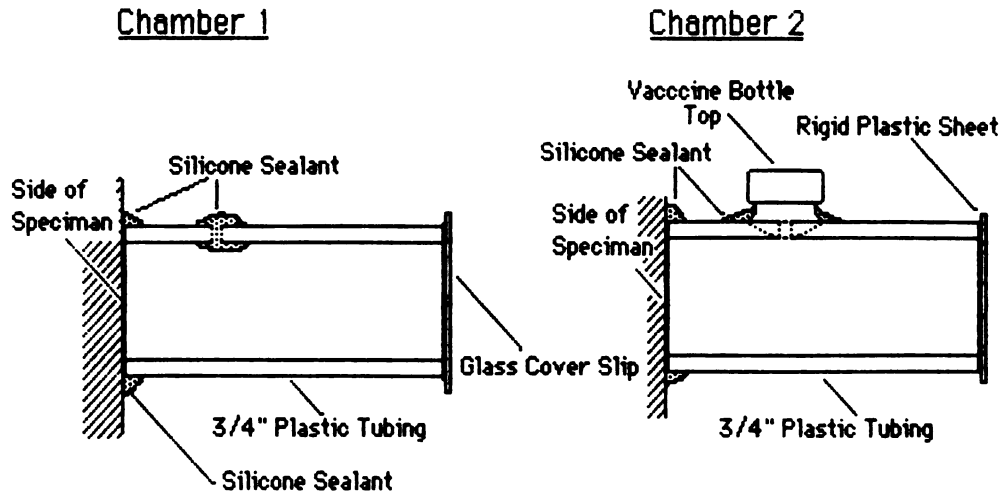


Figure [4.7] Environmental chambers 1 and 2.

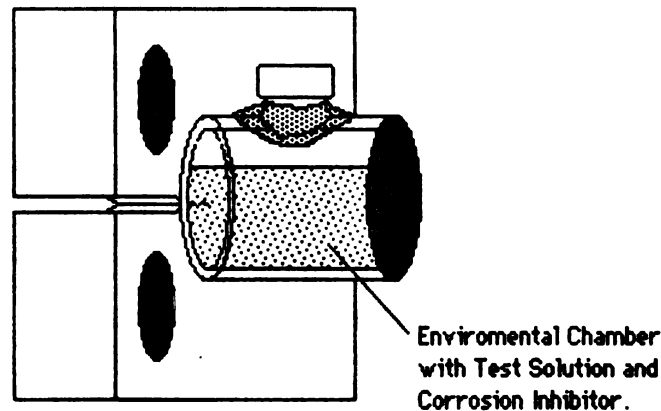


Figure [4.8] - Placement of the environmental chamber on the CTS.

Placement of the chamber on to the side of the specimen had to be very accurate. Because of the close proximity of the grips to the notch-end (where the environmental chamber had to be placed), the chamber had to be carefully mounted so as to barely overlap the notch-end but not the surface where the grip clevises would be. This worked out well, allowing the inhibitor to flow into the crack with ease but not into the precut notch. The portion of environmental chamber 2 that did overlap the

notch-end was sealed with silicone sealant. The inhibitor/distilled water in the chamber could only flow into the crack.

4.15 Cathetometer

The cathetometer provided, was a vertical cathetometer, a telescope-like device used to measure vertical displacements. However, the crack in the mounted specimen grew horizontally. To solve this problem a horizontal apparatus was constructed. The cathetometer's head (the scope, micrometer, and positioning clamp) was removed and then mounted on a standard 0.75" metal rod. Since the distance the crack was to grow during the experiment was less than the span of the micrometer, the 0.75" rod did not need to be incremented, nor, since the head was clamped in place, did a second stabilizing rod need to be added (the vertical cathetometer had a rod on which the head was mounted, as well as a rod to prevent rotation of the head).

The 0.75" rod was mounted in the horizontal position. A series of three pairs of parallel rods were used to mount the 0.75" horizontal rod; the first pair, connected to the load frame, the second perpendicular to the first, coming away from the load frame, and the third vertical pair, perpendicular to both the first and second, coming up from the floor to keep the 0.75" rod horizontal. The seven rods were clamped together and the 0.75" rod was leveled with a level. [see figure 4.9a and 4.9b].

At the beginning of the precracking stage, the head was positioned so that the micrometer was zeroed, and the positioning clamp locked when the crosshairs of the scope were at the head of the precut notch. The cathetometer was accurate down to 0.001 cm [0.00001 m].

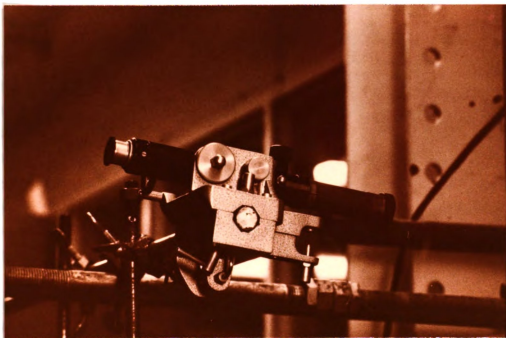


Figure [4.9a] Cathetometer Head.

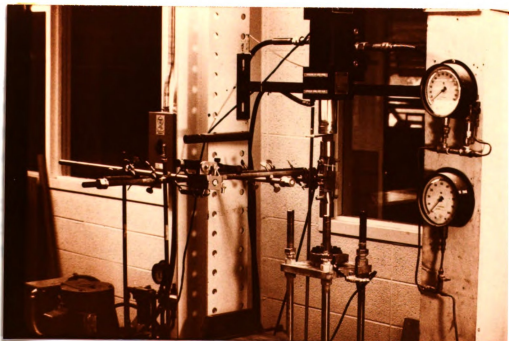


Figure [4.9b] Load frame with cathetometer mounting apparatus

4.16 Pretesting

After all of the testing apparatus was properly calibrated and put into place, a sample specimen was mounted in the grips and the individual pieces of equipment were checked to determine if their performance was adequate. During the equipment check chamber #1 was found to be unsuitable. In addition, it was discovered that the sides of the specimens needed to be polished before testing to enable accurate measurement of the crack length with the cathetometer. All minor equipment adjustments were made, chamber #2 was designed and built, and a sample test was run. After the sample test was performed, any further problems that arose were worked-out.

The sample test also showed that the specimen cracked nonuniformly across the cross section. This was the result of nonuniform loading. The uneven crack growth (and the nonuniform loading) was reduced by straightening the hydraulic ram and the platform, so that the specimen was being loaded closer to pure tension.

Section 4.2 - Method

4.21 Mechanical Analysis

The CF tests were similar to tests Khobaib performed at the Wright-Patterson AFB Facility. The MSU CTS's that were used in our tests were of a different configuration than those used in the Wright Patterson experiment. The load used in the Wright-Patterson experiments had to be converted to a stress value at the crack tip. The stress at the crack tip then could be converted back into a load value, for the same stress at the crack tip, but for a MSU CTS. Also, the load that was to be applied to MSU specimen during testing had to be less than the maximum load specified for the precracking stage.

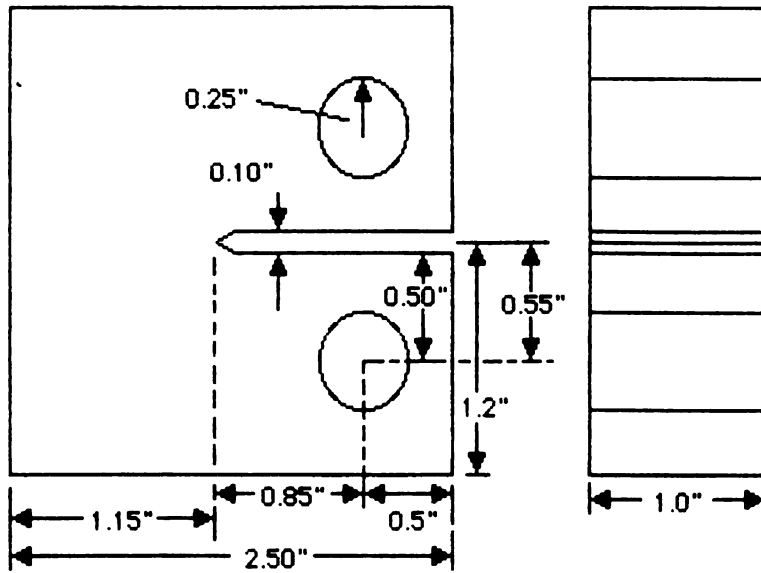


Figure [4.10] The Wright-Patterson Compact Tension Specimen.

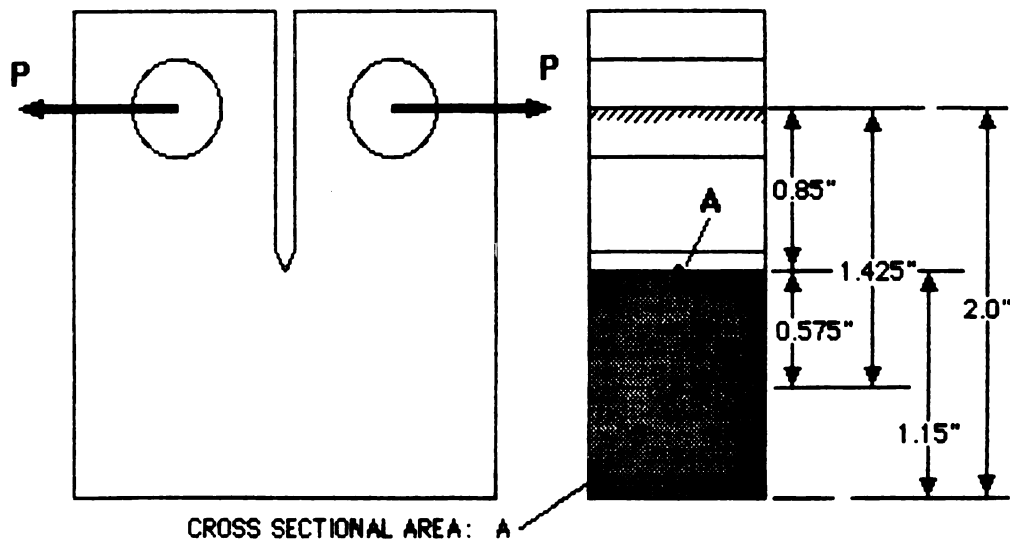


Figure [4.11] Wright-Patterson CTS.

Mechanical Analysis of the Wright-Patterson AFB specimen.

$$\sigma = \left(\frac{P}{A} + \frac{M y}{I} \right)$$

$$\sigma_A = \left(\frac{P}{1.15} + \frac{0.8194 P}{0.1267} \right)$$

$$\sigma_A = 7.34 P$$

Where:

$$M = [P R_c] = [1.425 P]$$

$$y = 0.575''$$

$$A = 1.15 \text{ in}^2$$

$$I = \frac{1}{12} b h^3 = (0.0833 \times 1.0 [1.15^3])$$

$$= 0.1267$$

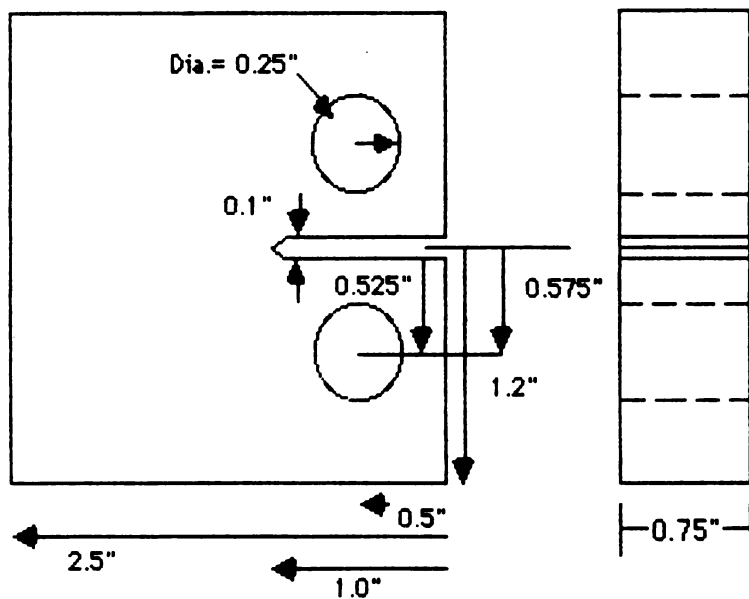


Figure [4.12] MSU Compact Tension Specimen.

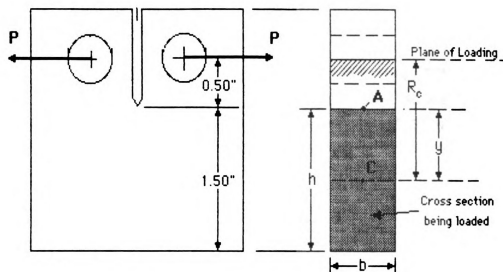


Figure [4.13] MSU Compact Tension Specimen

Mechanical analysis of the MSU CTS.

$$\sigma = \left(\frac{P}{A} + \frac{M y}{A \bar{y} (\bar{r} + y)} \right)$$

However, since the section shown above [see fig.3] is a symmetric section, a rectangle, the following equation can be applied.

$$\sigma = \left(\frac{P}{A} + \frac{M y}{I} \right)$$

Where:

$$M = [P R_c] = [1.25 P]$$

$$y = 0.75 \text{ in}^2$$

$$A = 0.75 \times 1.5 = 1.125 \text{ in}^2$$

$$I = \frac{1}{12} b h^3 = [0.0833 \times 0.75 \times (1.50)^3] \\ = 0.21094$$

$$\sigma_A = \left[\frac{P}{1.125} + \frac{0.9375P}{0.21094} \right]$$

$$\sigma_A = 5.33P$$

The mechanical analysis of the two specimens allowed calculation of the stress at the crack tip as a function of load. The load for the Wright-Patterson CTS could then be converted to a load for the MSU CTS specimen.

4.22 Conditions

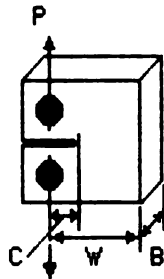
4.22a Precracking Conditions

For calculating the precracking conditions ASTM E399 was consulted and followed. The appropriate precrack load was determined from the maximum allowable stress intensity specified by the standard. The standard stated, that the maximum stress intensity in the terminal stages of precracking could not be greater than 60% of K_{IC} of the material¹.

Equation 1.0

$$K_I = \frac{P}{B W^{3/2}} \left(29.6 \left(\frac{C}{W} \right)^{3/2} - 185.5 \left(\frac{C}{W} \right)^{5/2} + 655.7 \left(\frac{C}{W} \right)^{7/2} - 1017 \left(\frac{C}{W} \right)^{9/2} + 639 \left(\frac{C}{W} \right)^{11/2} \right)$$

Where:



The K_{IC} minimum for 7075 T651 aluminum plate was 20 ksi $\sqrt{\text{in}}$ in the TL orientation and 25 Ksi $\sqrt{\text{in}}$ in the LT orientation (ASM). The K_I for the terminal portion of the precracking stage was to be less than 60% of K_{IC} ($0.6 \times 20 \text{ ksi} \sqrt{\text{in}} = 12 \text{ Ksi} \sqrt{\text{in}}$). The values of P, C, W, and B for the MSU CTS at the terminal point of precracking [considering a maximum precrack of 0.10"], were: C=0.60", W=2.0", B=0.75" (see the figure accompanying equation 1). Solving Eqn. [1] for load yielded $K_I = 5.526P$ (psi $\sqrt{\text{in}}$). If a load (P) of 2000lbs were used, $K_I = 11052 \text{ psi} \sqrt{\text{in}}$. A $K_I = 11052 \text{ psi} \sqrt{\text{in}}$ is less than 12 Ksi $\sqrt{\text{in}}$. A load of 2000lbs satisfied all the of the constraints set out in ASTM E-399 Sec. A2.1. Therefore, the load conditions for the precracking phase of the experiment were:

P (load)	2000 lbs.
Frequency	2 Hz.
R (Min. Load/Max. Load)	0.1
Waveform	Sinusoidal

Table [4.3] Precrack conditions.

A cyclic frequency of 2 Hz was chosen to provide a compromise between time efficient testing and accurate loading by the hydraulic ram. The experimental procedure used at the Wright-Patterson AFB Research facility specified a ratio, r [minimum stress (or Load)+maximum stress (or load)], of 0.1. The ratio ($r=0.1$) was within the limits specified in ASTM E399. Having fulfilled both requirements, $r = 0.1$ was used for both the precracking and experimental cycling phases.

4.22b Experimental Conditions

Comparing the specimen designs, it was specified that a load of 1200 lbs. was used in the tests at Wright-Patterson AFB. The mechanical analysis of the CTS used at Wright-Patterson AFB showed a mechanical advantage of 7.43 to 1. For a load of $P=1200$ lbs the stress at point A (see Figure [4.10]) would be 8808 psi. The MSU CTS yielded a mechanical advantage of 5.33 times the load. Thus the load necessary to produce the same stress (8808 psi) at point A in the MSU CTS would be 1652. lbs.. Therefore, the load for the experimental conditions was set between 1652 lbs. and 2000 lbs. (The load used in the precracking step), at 1700 lbs, producing a stress at the crack tip of 9061 psi. Note: the lower the load the less accurate the equipment because of the limits of the proving ring. Therefore, the higher load was used. The load conditions and the corresponding voltages, used by the controllers, for the experimental conditions were:

Maximum Load	1700 lbs	0.715 V
Minimum Load	170 lbs	0.071 V
Mean Load	935 lbs	0.393 V
Frequency	0.5 Hz	-
Waveform	Sinusiod	-

Table [4.4] Experimental conditions.

4.23 Specimen Preparation

The preparation of the specimen for the actual data gathering portion of the experiment consisted of several steps. The first, polishing both sides of the specimen in the area through which the crack would grow, was done to facilitate accuracy and convenient use of the cathetometer.

In trial runs, with unpolished specimens it was often difficult to determine the actual location of the crack tip. This caused the values of the crack growth rate to fluctuate more than they normally would under optimum measuring conditions. The specimen was polished with 600 grit paper until all marks even resembling the crack were totally eliminated.

4.24 Precracking Procedure

After the specimen was polished it was washed with water and then with distilled water and dried under an air jet. The specimen was then mounted in the grips and cycled under the precracking conditions:

P (load)	2000 lbs.
Frequency	2 Hz.
R (Min. Load/Max. Load)	0.1
Waveform	Sinusoidal

Table [4.5] Precrack conditions.

The specimens were cycled to a precrack length of 0.180 cm. During pretesting, it was found that a precrack of 0.10", as specified in similar experiments done on 7075- T6 aluminum at Wright-Patterson AFB,

was not necessary. The MSU CTS exhibited nearly constant mean crack growth rates soon after the experimental conditions were induced, therefore, there was no need to grow the crack any further before introducing the inhibitor into the environmental chamber. This may have been a result of geometry.

4.24a Chamber mounting

An intermediate step of the precracking process was chamber mounting. The specimens were precracked to a crack length of 0.15 cm [for the side with the longer crack], and the chamber was affixed to the specimen. Because the specimens did not precrack evenly, the side which the chamber was mounted on could affect the data. For the first specimen the environmental chamber was mounted to the side with the short crack, and the data was taken from the side with the longer crack. For the second and third specimens the chamber was mounted in the opposite fashion. Previous to being attached to the specimen, the chamber was washed with distilled water at least five times to remove any contaminants or inhibitor left behind from the previous experiment.

To mount the chamber, the specimen was removed from the grips and glued onto the selected side of the specimen with Dow Corning Silicone Sealant. The glue was allowed to dry. Once dry, the specimen was remounted in the grips and reloaded under the precrack conditions to a precrack length of 0.18 cm.

4.24b Solution Preparation

The inhibitor solution was to be introduced into the chamber using a syringe. The amount of inhibitor added was dictated by the amount of distilled water already in the chamber. There was some loss of distilled water through the crack as it opened and closed. This amount, however, was negligible compared with gross volume of the chamber. Further on in the experiment, when the crack opening was much greater and after the inhibitor solution had been introduced, there was minor solution loss through the crack opening.

The concentration of the inhibitor that was to be used was obtained from Lenz's thesis. The inhibitor was a sample obtained from the Erny Supply Co., Tampa Fl. The following weight percents were listed for

the components of the inhibitor:

<u>Compound</u>	<u>Weight %</u>
Borax	0.35
Sodium Nitrate	0.1
Sodium Nitrite	0.05
Silicate	0.01
Phosphate	0.002
<u>MBT</u>	<u>0.001</u>
Sum	0.513

Table [4.6] Inhibitor Composition.

The inhibitor was mixed in 500 ml batches. The inhibitor solution was mixed at double strength so it could be added directly to the distilled water already in the chamber. Therefore, instead of adding 5.13 grams of inhibitor to 1.0 liters of distilled water, 5.13 grams of inhibitor was added to 0.5 liters of distilled water. The double strength inhibitor/distilled water solution was stirred for a minimum of 45 min. with a magnetic stirrer.

4.25 Experimental Procedure

After the precracking step was completed, the specimen was unloaded and the load conditions were changed to the experimental load conditions. The following table lists the experimental conditions used:

Maximum Load	1700 lbs	0.715 V
Minimum Load	170 lbs	0.071 V
Mean Load	935 lbs	0.393 V
R(Min. Load/Max.Load)	0.1	-
Frequency	2 Hz	-
Waveform	Sinusiod	-

Table [4.7] Experimental Conditions.

Once the load conditions were set, the specimen was reloaded into the grips and distilled water was injected into the chamber through the syringe port using a 1 cc syringe. The usual amount of distilled water added was 4.0 to 4.5 cc [ml]. The amount of distilled water added to the chamber was dictated by the volume necessary to allow flow into the crack. The specimen was then cycled until it exhibited a constant mean crack growth rate.

The crack growth rate was constantly fluctuating around the mean crack growth rate. This could be attributed to the uneven crack growth across the specimen. The hydraulic ram was mounted in such a way that the stroke was not perfectly vertical. This resulted in uneven loading of the specimen across the cross section. The ram was adjusted as much as could be. The base was also adjusted to compensate as much as possible, but the system could not be fully straightened. Specimen number three exhibited the most uniform growth across the cross section of the specimen. It also displayed significantly less fluctuation in crack growth rate than did either of the other two other tests.

4.25a Introduction of Inhibitors

The concentration of the inhibitor injected into the chamber was double the regular concentration listed previously in this report. Therefore, instead of adding 5.13 grams of inhibitor to 1.0 liters of distilled water, 5.13 grams of inhibitor was added to 0.5 liters of distilled water.

The double concentration inhibitor solution was added to an equal volume of distilled water (already in the chamber) when the crack growth rate was constant. This yielded a standard concentration inhibitor

solution in the environmental chamber.

4.25b Termination

The specimen was then cycled until the crack growth rate was clearly reduced, and continued to show a fatigue crack growth rate below the rate previous to the introduction of the inhibitor. Once the specimens demonstrated the effect of the inhibitor on the crack growth rate, they were cycled to a crack length of at least 0.60 cm and then fractured. The specimens were then washed lightly with distilled water, lightly air jet dried, and placed in a dessicator.

Section 5.0 - Data

5.1 Data Conversion

There were three experiments. The quality of the experiments as well as the accuracy of the data recorded constantly improved. The two data values collected at intervals varying from 500 to 2500 cycles, were the crack length and the corresponding number of cycles. From the numerical data collected, two values were calculated for each pair. The first, the crack growth rate (da/dN), or the crack growth per cycle had units of m/cycle. The equation used to calculate da/dN was

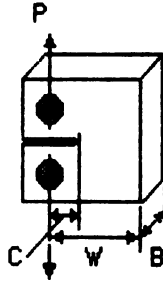
$$(a_{n+1} - a_n) / (N_{n+1} - N_n) = da/dN$$

where a_n = crack length [at data point n] in meters and N_n = number of cycles [at data point n].

The second value calculated was the stress intensity (units were $\text{MPa}\sqrt{\text{m}}$). Stress intensity is a function of the crack length, geometry of the specimen and load. The following equation was used to calculate stress intensity.

$$K_I = \frac{P}{B W^{3/2}} \left(29.6 \left(\frac{C}{W} \right)^{1/2} - 185.5 \left(\frac{C}{W} \right)^{3/2} + 655.7 \left(\frac{C}{W} \right)^{5/2} - 1017 \left(\frac{C}{W} \right)^{7/2} + 639 \left(\frac{C}{W} \right)^{9/2} \right)$$

Where:



For the experiment, the values of P, W, and B (P = 1700lbs [7561.6 N], W = 2in [0.0508 m], and B = 0.75in. [0.01905 m]) were constant, converting to...

$$K_I = 1.761 \left[29.6 \left(\frac{C}{0.0508} \right)^{1/2} - 185.5 \left(\frac{C}{0.0508} \right)^{3/2} + 655.7 \left(\frac{C}{0.0508} \right)^{5/2} - 1017 \left(\frac{C}{0.0508} \right)^{7/2} + 639 \left(\frac{C}{0.0508} \right)^{9/2} \right]$$

(MPa√m)

The value of C was equal to $(a_n + 0.0127)$, where a_n is the crack length in meters [at data point n] (0.0127m was the length of the precut notch).

5.2 Data

For the first test specimen, the side with the longer crack was monitored with the cathetometer. The side with the shorter crack had the environmental chamber mounted on it. The hydraulic ram was not as close to vertical as it was in the second and third experiment.

The performance of the inhibitor was not well displayed in this test. However, the average crack growth rate before the inhibitor was added was 2.94×10^{-7} m/cycle, and the average crack growth rate after the inhibitor was added was 2.44×10^{-7} m/cycle. The crack growth rate dropped 17% after the inhibitor was added.

A third order polynomial regression was fit to the data. Then both the data points and the plot of the third order polynomial were graphed using Statview™ software and an Apple Macintosh™ computer. Figure [5.1] shows the graph. The graph does not show the inhibitor as having a significant effect after being added. The fluctuations in the data made it difficult to obtain any clear conclusions from the first test. Though the aforementioned drop in the average crack growth rate may indicate a slight modification in crack growth behavior.

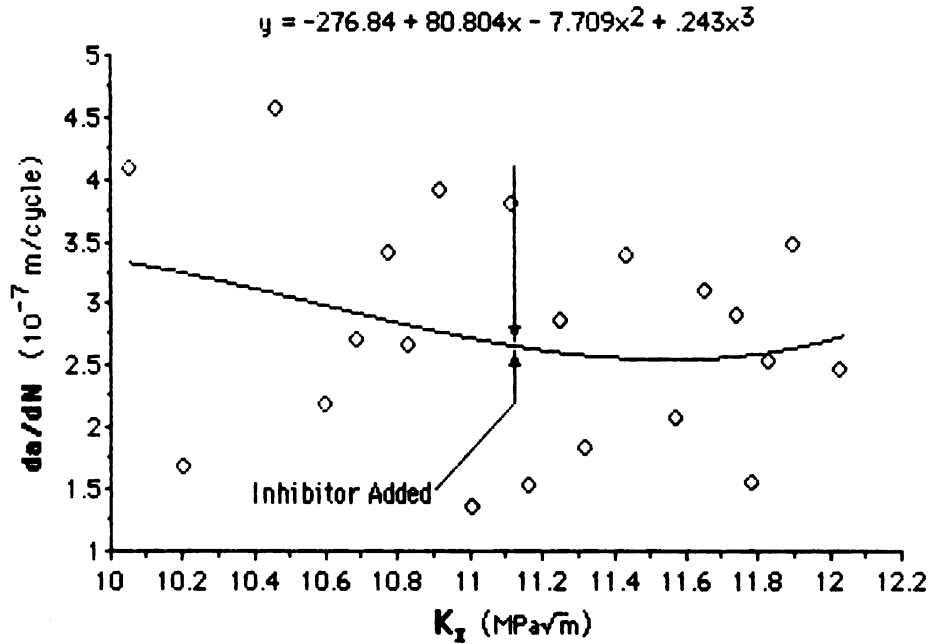


Figure [5.1] da/dN vs K_I plot for test No. 1.

The plot shows the data points, the curve produced by the third order polynomial regression, and the stress intensity level at which the inhibitor was added. The scatter of the data points was unsatisfactory, however the data did yield mean crack growth rates.

Before the second test was run, the platform on which the load cell (and thus the lower grip) was mounted was straightened. This change helped alleviate the uneven crack growth experienced in the first test. For the second test specimen, the side with the shorter crack was monitored with the cathetometer. The chamber was mounted on the side with the longer crack. In this test the inhibitor seemed to have a definite effect on the crack growth rate.

Again, a third order polynomial regression was fit to the data. The polynomial regression and data were plotted. Figure [5.2] shows that there was a drop in the crack growth rate almost immediately after the inhibitor was added. The delay might be the result of a slow, steady increase in the crack growth rate prior to the introduction of the inhibitor, or the time of diffusion of the inhibitor to the crack tip.

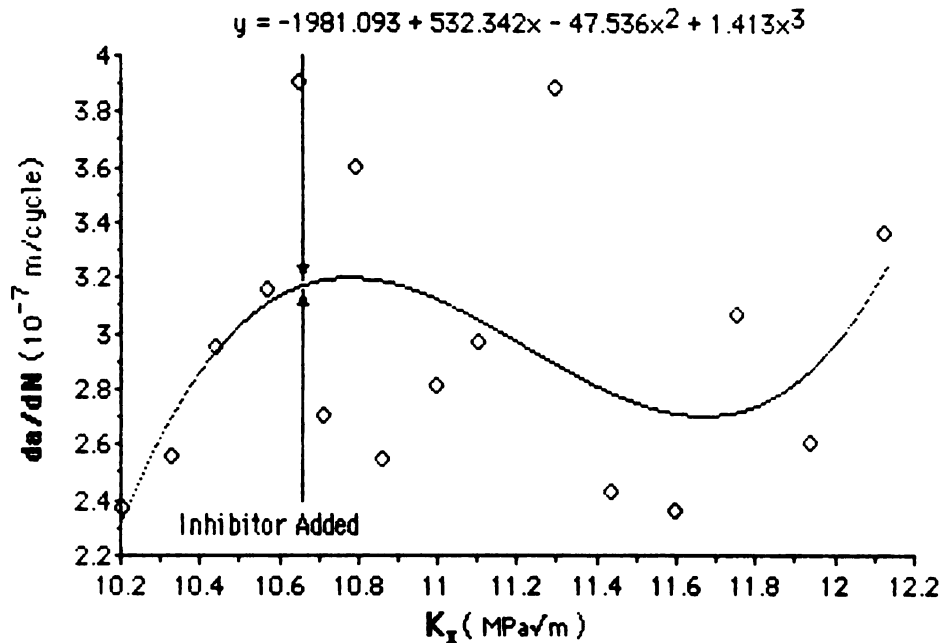


Figure [5.2] da/dN vs K_I plot for test No. 2.

The above plot shows the data points, the curve produced by the third order polynomial regression, and the stress intensity level at which the inhibitor was added. The graph shows a drop in the crack growth rate at approximately 10.75 MPa \sqrt{m} , soon after the inhibitor was added at 10.65 MPa \sqrt{m} .

Once again the platform was aligned to both tighten and straighten. The alignment was the closest to vertical that had been achieved. For test specimen 3, the side with shorter crack was monitored with the cathetometer and the side with the longer crack had the environmental chamber mounted on it. Unlike the first two tests, test specimen 3 cracked nearly evenly across the cross section. This did have a positive effect on the magnitude of fluctuations of the crack growth rate during the experiment. Again a polynomial regression was fit to the data, however, a fourth order polynomial was used. The polynomial plot and data points were graphed. The plot shown in Figure [5.3] shows the crack growth rate dropped immediately after the inhibitor was added, displaying a second time that the inhibitor does have an effect on the crack growth rate.

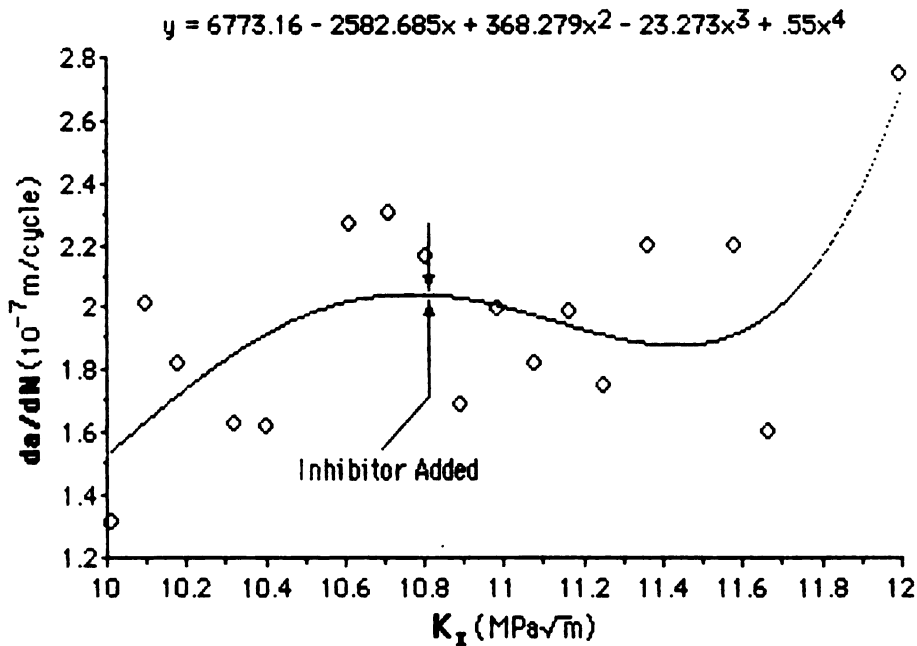


Figure [5.2] da/dN vs K_I plot for test No. 2.

The above plot shows the data points, the curve produced by the third order polynomial regression, and the stress intensity level at which the inhibitor was added. The graph shows an immediate drop in the crack growth rate after the inhibitor was added at a stress intensity of 10.8 MPa√m.

Because the crack growth across the specimen was more even in the third experimental run, the data is more likely to be representative of the actual performance of the inhibitor.

5.3 Discussion of Data

In comparison with the data obtained by Kobaib, the effects of the inhibitor in slowing corrosion fatigue crack growth rates were not nearly as dramatic. However, the plot (Figure [3.1]) showing the effects of various environments on crack growth rates of Al 7075-T6 shows that distilled water is less aggressive and less severe than the 0.1M NaCl solution. In the following figure (Figure [3.2]) it shows that the crack growth rates of both the distilled water and 0.1M NaCl solution in the presence of the inhibitor are nearly identical. Therefore, the effect the inhibitor would have on a growing crack in distilled water would also be

much less pronounced than in the presence of the sodium chloride.

5.4 SEM Evaluation

An analysis of the fracture surface showed a similar relationship. The fracture surface exposed to only distilled water, shown in Figure [5.4] and [5.5] exhibited less evidence of normal fatigue behavior. The surface showed some brittle shear. Whereas the surface where the crack grew in the presence of the inhibitor, Figure [5.6] and [5.7] had reduced brittle shear features and more normal fatigue features. Once again the effects that the inhibitor had in the presence of distilled water were not as dramatic as those displayed in Khobaib's research. This is again the result of the less aggressive nature of the distilled water compared to sodium chloride.

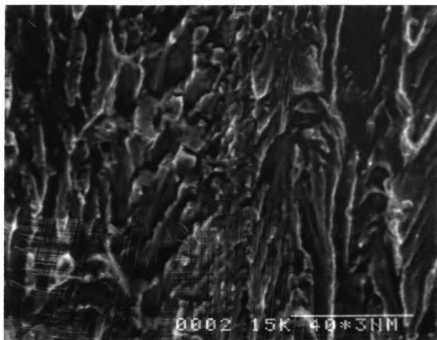


Figure [5.4] CF Fracture surface without inhibitor 750x.

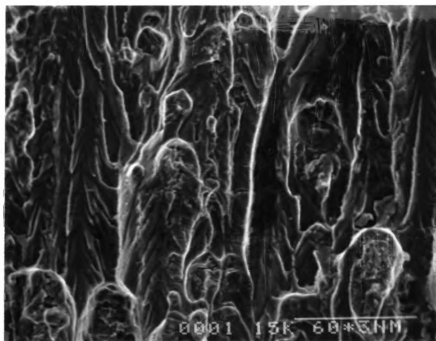


Figure [5.5] CF fracture surface without inhibitor 500x.

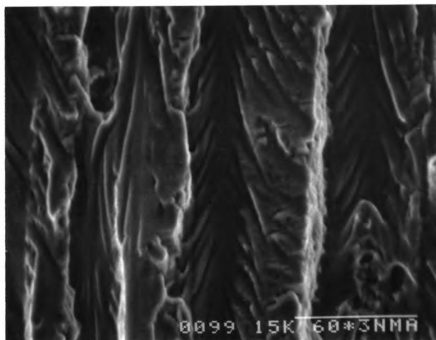


Figure [5.6] CF fracture surface in the presence of inhibitor 1000x.

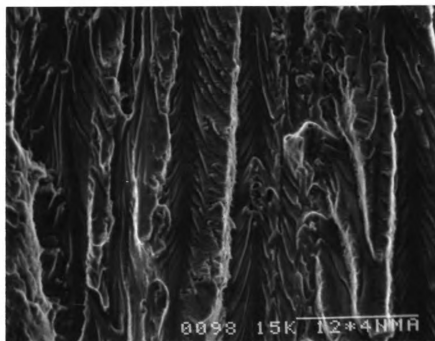


Figure [5.7] CF fracture surface with inhibitor 500x.

6.0 Conclusions

1) The data shows that the inhibitor had a positive effect on the corrosion fatigue behavior of 7075-T651 Al. Both the da/dN vs K_I plots and the SEM fractographs showed that the inhibitor retarded the accelerating effect of the distilled water. In addition, the experimental results showed the system is functional. The experiment data displayed that further refinements in technique need to happen before comparative results can be accurate.

2) Further improvements in experimental techniques could yield more accurate results. Among the improvements made the most influential would be to reduce the fluctuations in the crack growth rate. This could be done most effectively by aligning the ram and the lower platform so that the displacement of the ram is perfectly vertical in relation to the specimen. An other possible area that could be looked into would be the rate, gain, and delta P controls on the MTS 406.11 unit. In addition, the crack might be allowed to grow further into specimen (region II of the da/dN vs K_I curve) before adding the inhibitor. However this might prove useless, because the fluctuation of the crack growth rate was no less with increased crack lengths. As more experiments are run, the quality of the data collected should continue to improve.

3) The next logical step in the research program would be to continue use of the testing apparatus to evaluate the effects of the inhibitor in a NaCl solution and to attempt to reproduce Khobaib's results (see Figure [K6]). Then the system can be used to evaluate new inhibitor formulations.

Bibliography

1. 1984 Annual Book of ASTM Standards, vol 03.01, ASTM E 399, 1984.
2. "Selection: Nonferrous Alloys and Pure Metals", ASM Materials Handbook Ninth ed. pp 59-62, 129-132, American Society for Metals, 1979.
3. F.P. Beer, E.R. Johnston, Jr., Mechanics of Materials, McGraw Hill, 1981.
5. K.J. Bhansali, C.T. Lynch, R. Summitt, F.W. Vahldiek, "Inhibition of Environmentally Enhanced Crack Growth Rates in High Strength Steels", reprinted from Environment-Sensitive Fracture of Engineering Materials, Proceedings of Symp. TMS-AIME, Chicago., Fall, 1977.
6. F. Castellanos, Effects of Surfactants Upon Corrosion Inhibition of High-Strength 7075-T6 Aluminum, pp 1, 2, 50-53, Michigan State University, 1985.
7. M. Cohen, "The Breakdown and Repair of Inhibitive Films in Neutral Solutions", Corrosion 32, pp 461-465, 1976.
8. G.E. Dieter, Mechanical Metallurgy-Materials Science and Engineering Series, McGraw Hill, 1976.
9. D.J. Duquette, "Environmental Effects I: General Fatigue Resistance and Crack Nucleation in Metals and Alloys", Fatigue and Microstructure, pp 345-359, American Society for Metals, 1979.
10. M. Khobalib, Accelerated Corrosion Testing - AFWAL-TR-82-4186, Wright-Patterson AFB, 1982.

11. M. Khobaib, C.T. Lynch, L. Quackenbush, "Effects of Surfactants Upon Corrosion Inhibition of High-Strength steels and Aluminum Alloys", Corrosion **39**, 253-257, 1983.
12. M. Khobaib, C.T. Lynch, F.W. Vahldiek, "Inhibition of Corrosion Fatigue in High Strength Aluminum Alloys", NACE, vol. 36, No. 5, May 1981.
13. M. Khobaib, C.T. Lynch, F.W. Vahldiek, "New Concepts In Multifunctional Corrosion Inhibition For Aircraft and Other Systems" - AGARD Conference Proceeding No. 315, Aircraft Corrosion, 1981.
14. M. Khobaib, Material Evaluation: Part II - Development of Corrosion Inhibitors - AFML-TR-79-4127, Wright-Patterson AFB, 1979.
15. K.B. Lenz, Corrosion in Aircraft - The Effects of Environment and Maintenance Operations - Masters thesis, pp 60-91, Michigan State University, 1985.
16. K.B. Lenz, R. Summitt, PACER LIME: Environmental Corrosivity: Non-CONUS Airbases. AFWAL-TR-84-XXXX, Michigan State University, 1985.
17. H.L. Marcus, "Environmental EffectsII: Fatigue-Crack Growth in Metals and Alloys", Fatigue and Microstructure, pp. 369-381, American Society for Metals, 1979.
18. Y.N. Mikhailovski, V.M. Popova, T.I. Sokolova, "Mechanism of Retardation of Corrosion of Iron by Oxygen-Containing Inhibitors of the Oxidizing Type: Chromates", Z. Metall. **19**, pp. 707-716, 1983.
19. J. Meiner, D. Schoener, Evaluation Of Inhibitors - Senior Thesis, Michigan State University, 1984.

20. H. Omura, Effect of Multi-Functional Inhibitors on the Electrochemistry Within a Corrosion Crack - Dissertation, Michigan State University, 1984.
21. R.M. Pelloux, R.E. Stolz, "Inhibition of Corrosion Fatigue in 7075 Aluminum Alloys", Corrosion-NACE 29, 13-17, 1973.
22. I.L. Rosenfeld, I.K. Marshkoo, Corrosion 20, 115 t, 1964.
23. R. Summitt, The Efficacy of Fresh Water Rinsing in Corrosion Control of Aircraft, Michigan State University, 1985.
24. R. Summitt, Inhibiting Corrosion Cracking: Crack Tip Chemistry and Physics, Michigan State University, 1986.
25. R. Summitt, Personnel communication, 5-14-86.
26. J.M. West, Basic Corrosion and Oxidation, pp102-103,109, Ellis Horwood, 1980.
27. N. Pourbaix, "Atlas of Electrochemical in Aqueous Solutions", NACE, Houston, p. 499, 1966.

MICHIGAN STATE UNIVERSITY LIBRARIES



3 1293 03169 3942